Rationally Designed Polyhedral Carbon Framework from Solid to Hollow for Long Cycle Life Secondary Battery

Zheng Zhang[a], Ying Huang[1a], Xiang Li[a], Xiaogang Gao[a], Panbo Liu[a], Tiehu Li[b]

(a) MOE Key Laboratory of Material Physics and Chemistry under Extraordinary Conditions, School of Chemistry and Chemical Engineering, Northwestern Polytechnical University, Xi'an 710072, PR China.

(b) School of Materials Science and Engineering, Northwestern Polytechnical University, Xi'an 710072, China.

[1] Corresponding author. Tel: +86 13909230894. E-mail address: yingh@nwpu.edu.cn (Ying Huang).

Experimental

preparation of ZIF-8@ZIF-67 precursors

Synthesis of ZIF-8, solution A (100 mL of methanol solution with 16 mmol 2-methylimidazole (2-MeIm)) was rapidly poured into solution B (100 mL of methanol solution with 8 mmol of completely dissolved $Zn(NO_3)_2 \cdot 6H_2O$) under magnetically stirring for 5 min and then aged for 24 h at room temperature. The as-prepared ZIF-8 precursor was by centrifugation, washed several times with methanol, and dried at 80 °C overnight for further using. Similarly, the ZIF-67 precursor was obtained with the same procedure in which $Zn(NO_3)_2 \cdot 6H_2O$ was replaced by $Co(NO_3)_2 \cdot 6H_2O$.

Synthesis of ZIF-8@ZIF-67 core-shell polyhedrons, 320 mg ZIF-8 were firstly dispersed in 40 mL of methanol for 30 min with ultrasonic assistance. Then, 10 mL of methanol solution with 3 mmol $Co(NO_3)_2 \cdot 6H_2O$ was added into the ZIF-8 suspension, kept stirring for another 30 min. Finally, 10 mL of methanol solution with 30 mmol 2-MeIm was rapidly poured into the above solution. After the final mixture was kept for 24 h at room temperature, brilliant purple ZIF-8@ZIF-67 precursors, washed several times with methanol, were harvested.

Preparation of polyhedron carbon framework

The obtained precursors were carbonized at 480 ℃, 650 ℃, 800 ℃, and 1000 ℃ for 3 h, respectively, with a ramp rate of 2 ℃/min under an H_2/Ar (volume ratio 1:9) atmosphere. Finally, the obtained black powders were collected and soaked into 6 M H_2SO_4 solution for 12 h to remove the Co and Zn nanoparticles. The resulting products were collected by centrifugation and repeatedly washed with deionized water before being dried at 80 ℃ overnight. The products were denoted as

PCF-480, PCF-650, PCF-800, PCF-1000.

Preparation of modified separators

80% PCF, 10% Super P and 10% polyvinylidene fluoride (PVDF) were mixed in N-methyl-2-pyrrolidone (NMP) solvent and stirred for a certain time to make a uniform slurry. The slurry was coated on a commercial polypropylene separator (Celgard 2400, PP) by doctor blade coating with negative-pressure infiltrating, drying at 40 ℃ overnight. And the as-prepared modified PP were named as PCF-x@PP (where x = 480, 650, 800, 1000, respectively).

Preparation of working electrode

In LSBs, the sulfur cathode was prepared by a melting diffusion method. Sulfur and CNT (8:2 mass ratio, denoted as S/CNT) were grinded in an agate mortar, after mixing evenly, transferred into a sealed container, heated to 155 ℃ for 12 h under an Ar atmosphere. The working electrode was prepared by mixing S/CNT with Super P and PVDF (mass ratio = 8:1:1) in NMP solution. The slurries were coated onto Al foil and dried at 60 ℃ overnight.

In LIBs and SIBs, the working electrode was prepared by mixing 70% PCF, 20% Super P, 10% PVDF and the obtained mixture was dispersed in NMP solution. Then, the slurry was subsequently brushed on copper foil and dried at 100 ℃ for 12 h in a vacuum box. Mass loading of active materials was 1.5~1.7 mg cm^{-2}.

Material characterization

X-ray diffraction analysis (XRD Rigaku, Cu Kα, Scan range of 5°-85°) detect the crystal structure of synthetic samples. The morphology and structure of the sample were observed using field emission scanning electron microscopy (FESEM FEI Verios G4) and transmission electron

microscope (TEM FEI Talos F200X TEM), and X-ray Photoelectron Spectroscopy (XPS) was used to detect the surface composition of the sample. The specific surface area and pore size distribution of the as-prepared material were tested by nitrogen adsorption/desorption. Raman spectra were determined using WlTec Alha300R Raman spectroscopy with a 532 nm laser. Thermogravimetric analysis (TGA, Netzsch STA 449 C) was implemented under N_2 atmosphere with a heating rate of 10 °C min^{-1}.

Electrochemical measurements

All batteries are assembled in the glove box with CR 2016 coin cells. To assemble LSBs, the lithium is the counter electrode, the separators is PCF-x@PP and commercial PP, the electrolyte was composed of 1.0 mol/L lithium bis(trifluoromethanesulfonyl)imide (LiTFSI) dissolved in a mixed solvent of 1,3-dioxolane (DOL) and 1,2-dimethoxyethane (DME) (1:1, w/w) with 2.0 wt.% of $LiNO_3$ as an additive. Cyclic voltammetry (CV) test with a voltage window of 1.7-2.8 V and electrochemical impedance spectroscopy (EIS) test with a frequency range of 100 kHz to 0.1 Hz were recorded on electrochemical workstation (USA GMARY Co). The galvanostatic charge/discharge measurements were performed between 1.7 V and 2.8 V by using a battery testing station (Land T2001A).

To assemble LIBs, the lithium is the counter electrode, the polypropylene film (Celgard 2400) is the separator, and the electrolyte is 1 M $LiPF_6$ dissolved in ethylene carbonate (EC), dimethyl carbonate (DMC) and diethyl carbonate (DEC) (1:1:1 w/w/w). To assemble SIBs, sodium metal foil as counter electrode, glass fiber film (Whatman GF/D) was used as separator, the electrolyte1 is 1 M $NaClO_4$ in propylene carbonate (PC) and ethylene carbonate (EC) (1:1, w/w) with the addition of

5 wt.% fluoroethylene carbonate (FEC). Cyclic voltammetry (CV) test with a voltage window of 0.01-3.0 V and electrochemical impedance spectroscopy (EIS) test with a frequency range of 100 kHz to 0.1 Hz were recorded on electrochemical workstation. The galvanostatic charge/discharge measurements were performed between 0.01 V and 3.0 V by using a battery testing station (Land T2001A).

Calculation of capacitance contribution

Electrochemical kinetics were analyzed by CV measurements at different scan rates from 0.1 to 1.0 mV s^{-1} and the measured current (i) and scan rate (v) obeyed the following relationship:

$$i = av^b \ \ and \log(i) = b \times \log(v) + log(a) \quad (1)$$

Where i is the current, v is the scan rates, and a, b are adjustable parameters. When the b value is close to 1.0, the process is controlled by a capacitive process. When the b value is close to 0.5, the process is controlled by diffusion. The capacitance contribution can be further quantified by the following formula:

$$i(V) = k_1 v + k_2 v^{1/2} \ or \ i/v^{1/2} = k_1 v^{1/2} + k_2 \quad (2)$$

k_1 and k_2 are constants. $k_1 v$ represents the contribution of capacitance control, while $k_2 v^{1/2}$ represents the contribution of diffusion control.

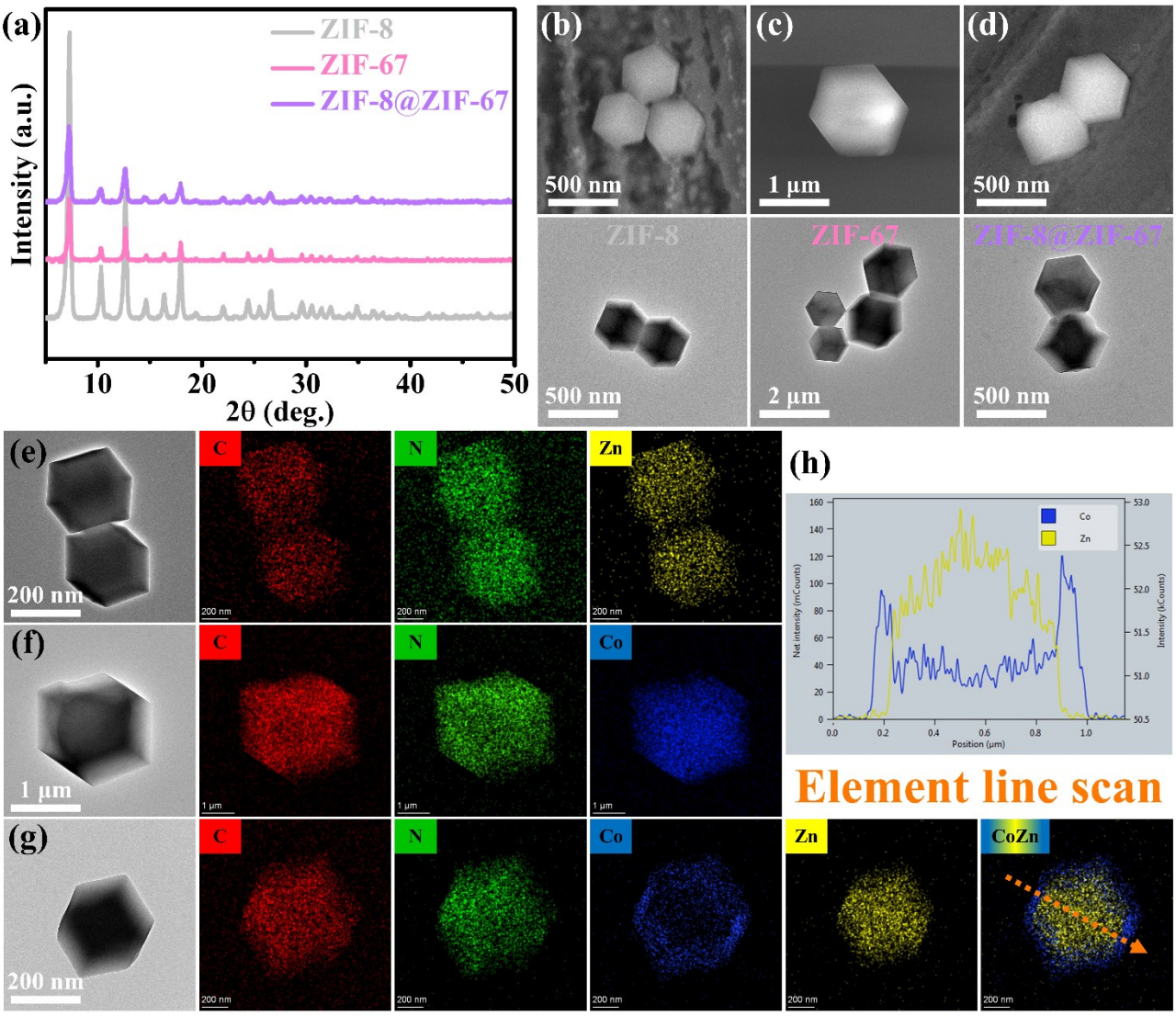

Figure S1. (a) XRD spectra of ZIF precursor. FESEM and TEM images of (b) ZIF-8, (c) ZIF-67, (d) ZIF-8@ZIF-67. EDS mapping of (e) ZIF-8, (f) ZIF-67, (g) ZIF-8@ZIF-67. Element line scan of ZIF-8@ZIF-67.

Table S1 Elemental composition analysis by XPS.

Materials	Carbon/at%	Nitrogen/at%	Oxygen/at%	Cobalt/at%
PCF-480	84.06	9.15	6.32	0.47
PCF-650	85.68	8.11	5.82	0.39
PCF-800	88.78	7.73	3.20	0.29
PCF-1000	92.16	4.58	3.07	0.19

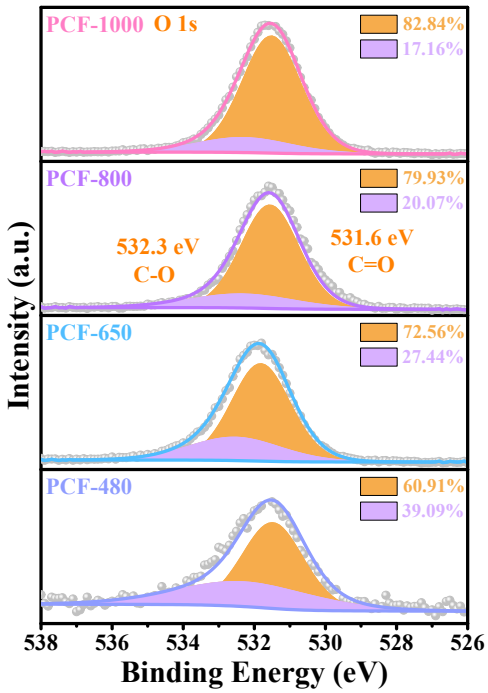

Figure S2. XPS spectra of O 1s.

Table S2 Specific surface area and pore volume of PCF at different temperatures.

Materials	PCF-480	PCF-650	PCF-800	PCF-1000
Specific surface area ($m^2 g^{-1}$)	38.675	311.340	566.300	499.880
pore volume ($cm^3 g^{-1}$)	0.135	0.391	0.720	0.598

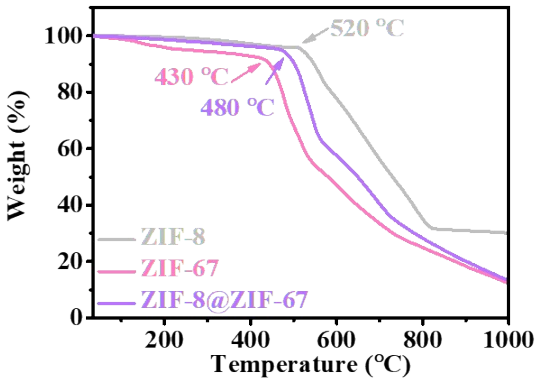

Figure S3. TG curves of ZIF-precursor.

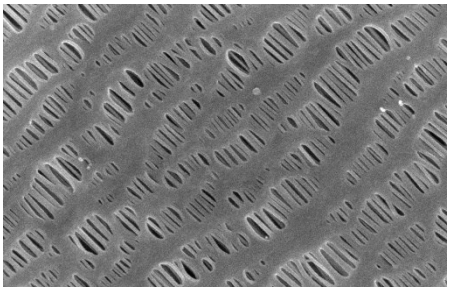

Figure S4. FESEM images of PP separator.

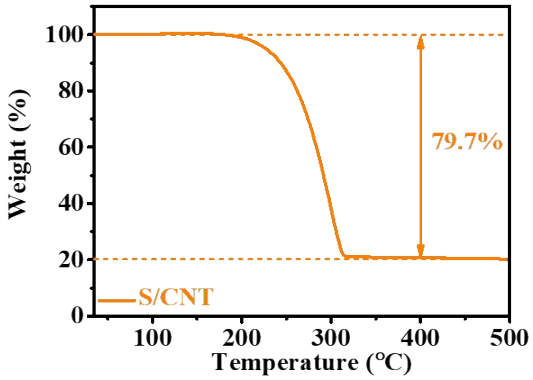

Figure S5. TG curves of S/CNT.

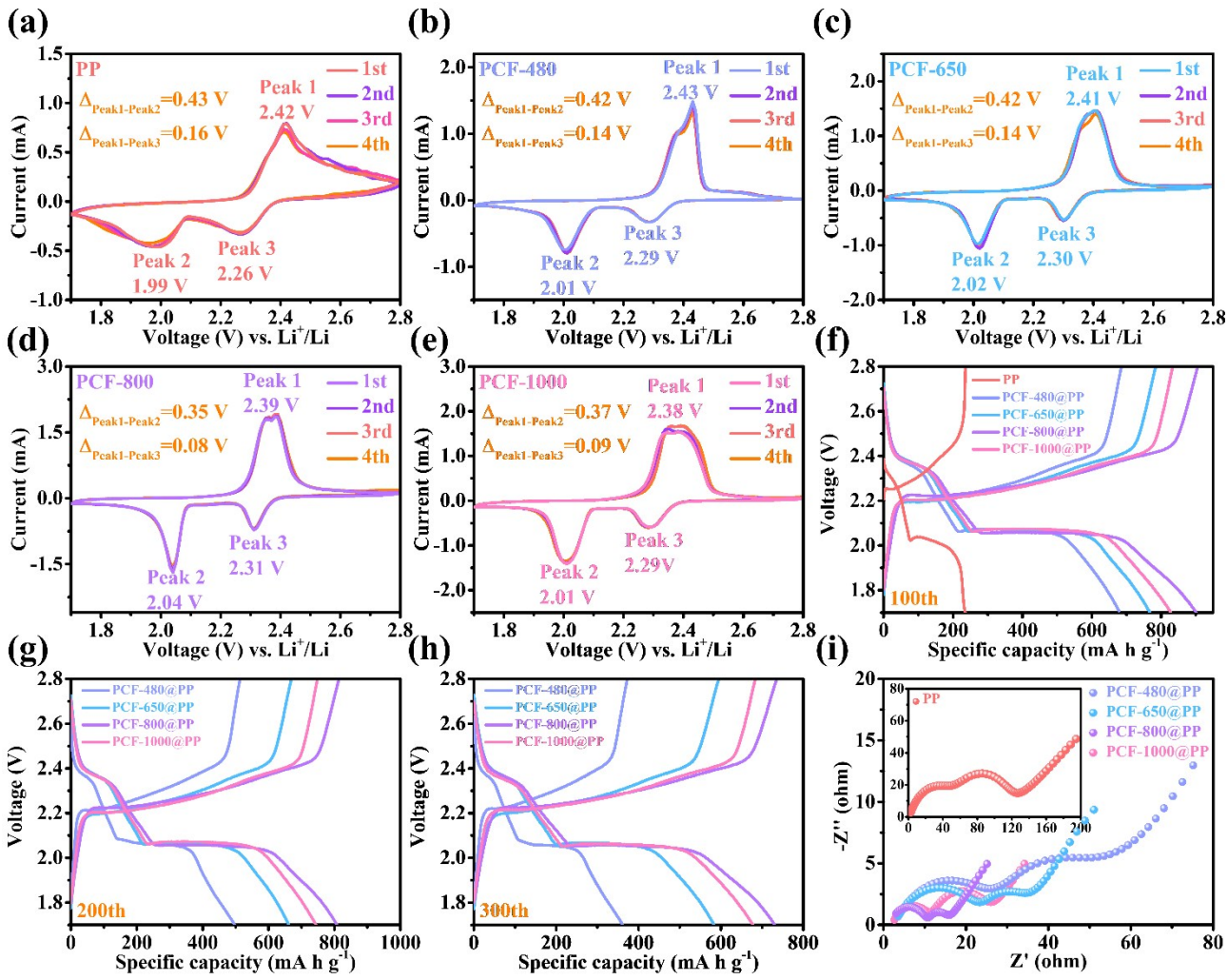

Figure S6. CV curves of (a) PP, (b) PCF-480, (c) PCF-650, (d) PCF-800, (e) PCF-1000. Galvanostatic charge/discharge curves of LSBs with different separators (f) 100th, (g) 200th, (h) 300 th. (i) EIS curves after cycling.

Table S3 Fitting values of the Rs, Rsei, and Rct at different conditions.

Separators	Rs	Rsei	Rct
PP before cycling	4.33	17.97	19.17
PCF-480@PP before cycling	2.42	12.48	7.24
PCF-650@PP before cycling	2.45	11.94	7.46
PCF-800@PP before cycling	2.25	4.12	4.04
PCF-1000@PP before cycling	2.26	3.46	4.03
PP after cycling	5.88	51.54	59.13
PCF-480@PP after cycling	2.55	21.12	33.28
PCF-650@PP after cycling	2.49	18.85	19.65
PCF-800@PP after cycling	2.22	8.15	4.96
PCF-1000@PP after cycling	2.25	11.16	14.67

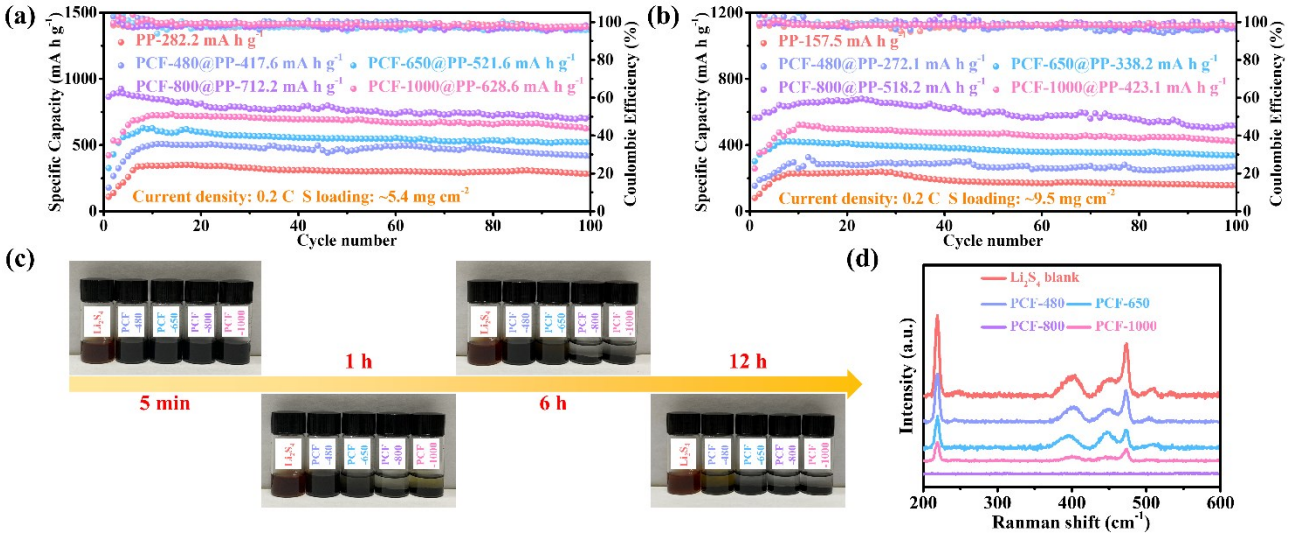

Figure S7. (a,b) Cycling performances of PCF@PP at 0.2 C with high area sulfur loading. (c) Static adsorption (d) Raman spectra of the Li_2S_4 solution and the supernatant solution after static adsorption 1 h.

The static adsorption test was studied by adding PCF to the red-brown Li_2S_4 solution. As shown in **Figure S7c**, after standing for 1 h, the Li_2S_4 solution of PCF-800 became colorless. After standing for 6 h, the Li_2S_4 solution of PCF-1000 also became colorless. After standing for 12 h, the Li_2S_4 solution of PCF-650 also became colorless. The PCF-480 solution is still slightly yellow even after being left for 12 h, but it is lighter than the original Li_2S_4 solution, indicating that there is a certain adsorption effect. This phenomenon shows that PCF-800 has a fast adsorption effect. In addition, the supernatant of the solution after the adsorption test for 1 h was taken for the Raman test (**Figure S7d**). The decrease of the peak intensity in the Raman spectrum further proves the effective interaction between Li_2S_4 and PCF-800.

Table S4 Comparison of the cycling performance of this work with previous report related to the modified separator.

Modified separator	Thickness (μm)	Cathode (sulfur content wt%)	Sulfur loading (mg cm^{-2})	Current rate (C)	Capacity (mAh g^{-1})	Cycle life (cycles)	Capacity decay rate
CNT/ Al_2O_3@PP	18/10	CNTs/S (70%)	1.0-1.2	0.2	760.4	100	0.306%
Fe_3C-N-rGO@PP[1]	10	S/SP (60%)	0.7-1	0.5	722.1	100	0.068%
Red phosphorus@PP[2]	8	C-S (80%)	2.0	1.0	729.6	500	0.036%
$Ni_3(HITP)_2$@PP[3]	8	S/SP (60%)	-	0.5	585.4	300	-
PEI/fish-scale based porous carbon@PP[4]	6	S/AB (63%)	1.5	1.0	683.0	400	0.030%
ZnO/graphene@PP[5]	71.2	C-S (70%)	1.1–1.5	1.0 2.0	641.6 764.9	500 300	-
CoP/C@PP[6]	17.7	KB/S (75%)	1.4	1.0	562.0	500	0.08%
CNFs-VS_4@PP[7]	10	CB/S (80%)	1.0-1.5	2.0	520.0	600	0.07%
AC/Ni/N@PP[8]	17	CB/S (80%)	2.0	1.5	575.0	700	0.049%
PCF-800@PP (This work)	10.6	CNTs/S (80%)	1.2	1.0	625.4	1000	0.046%

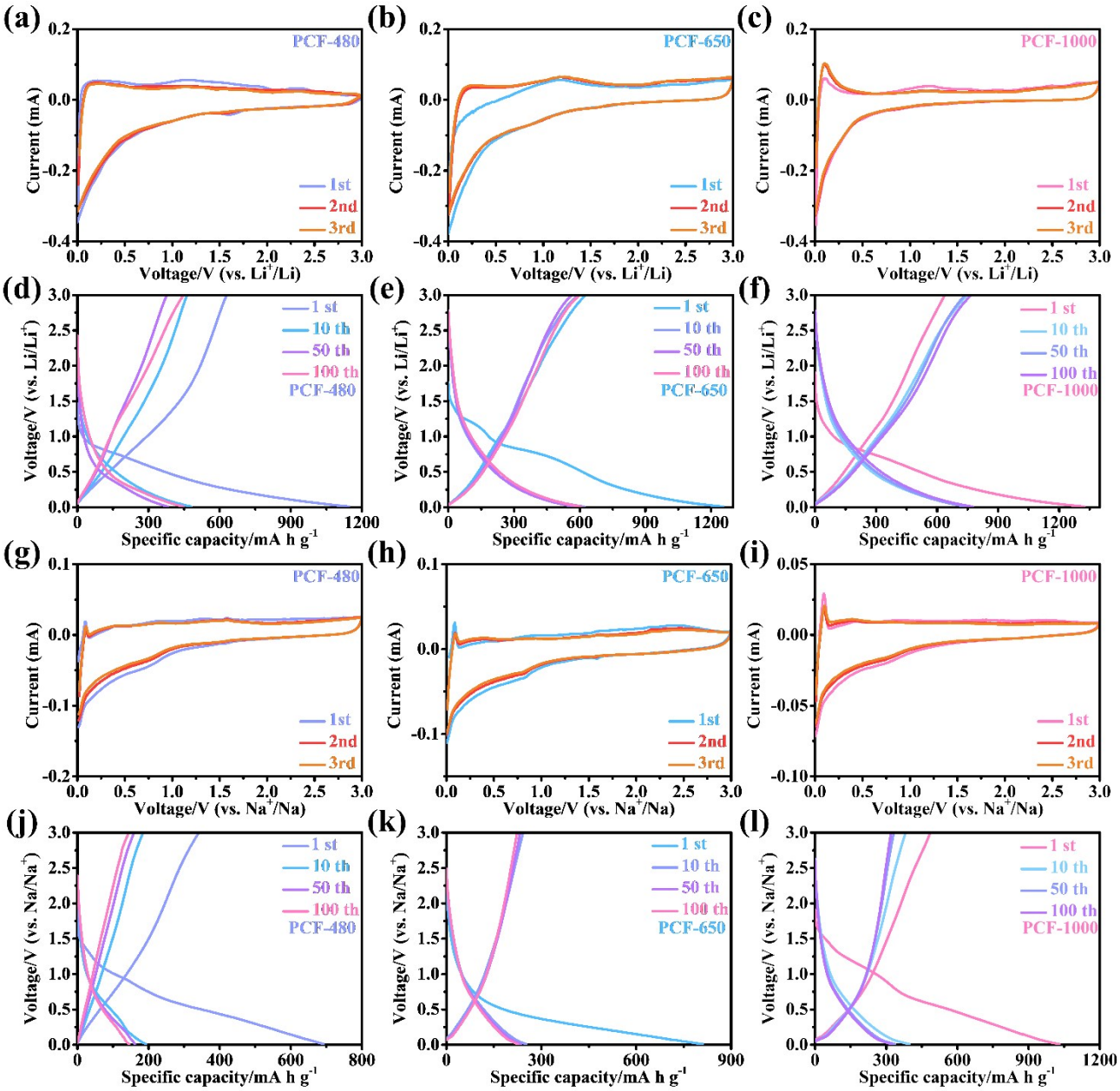

Figure S8. (a-l) CV and GCD curves of PCF for LIBs and SIBs.

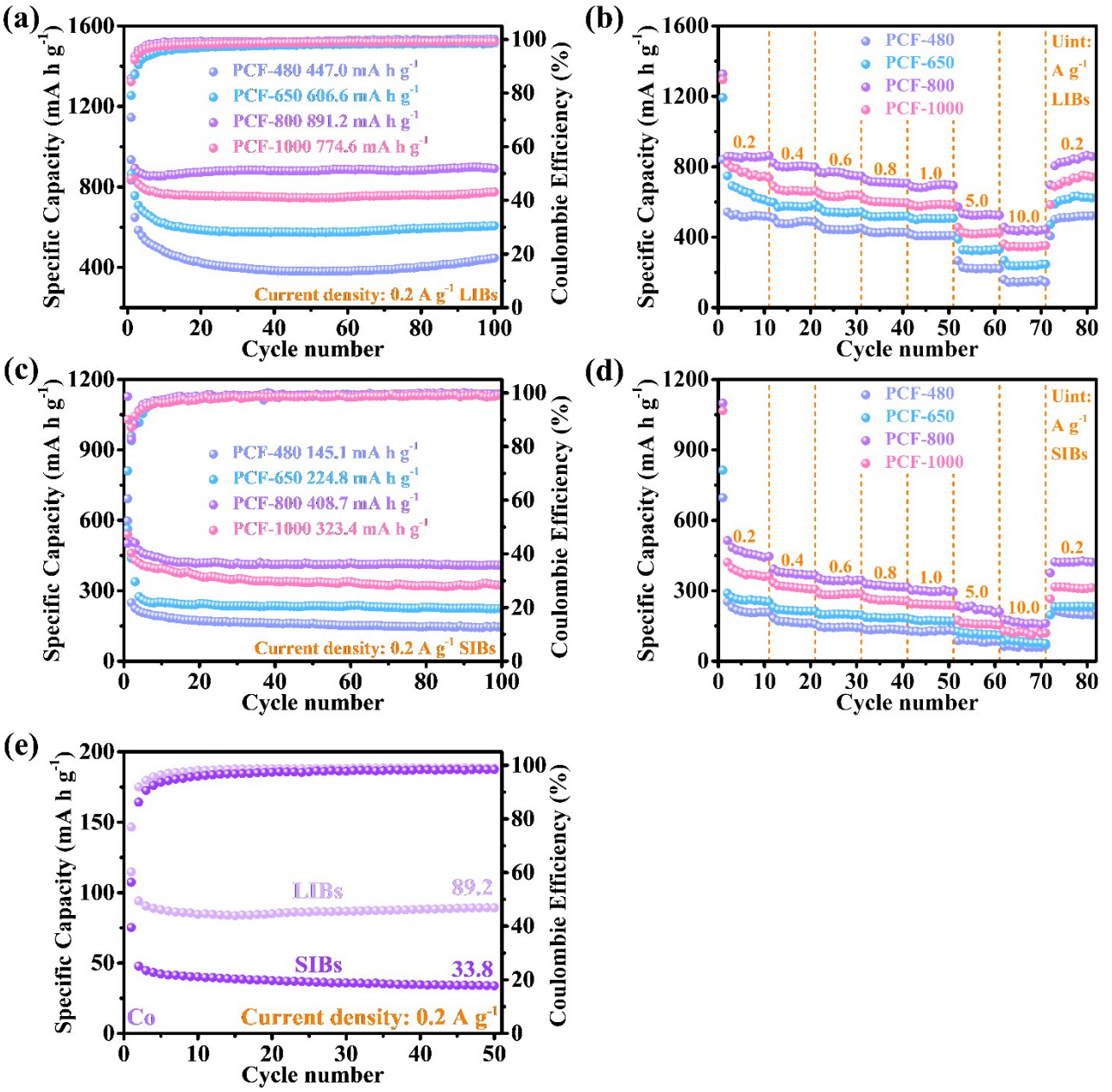

Figure S9. (a,c) Cycling performances of PCF at 0.2 A g^{-1} and (b,d) rate performances. (e) Cycling performances of Co at 0.2 A g^{-1}.

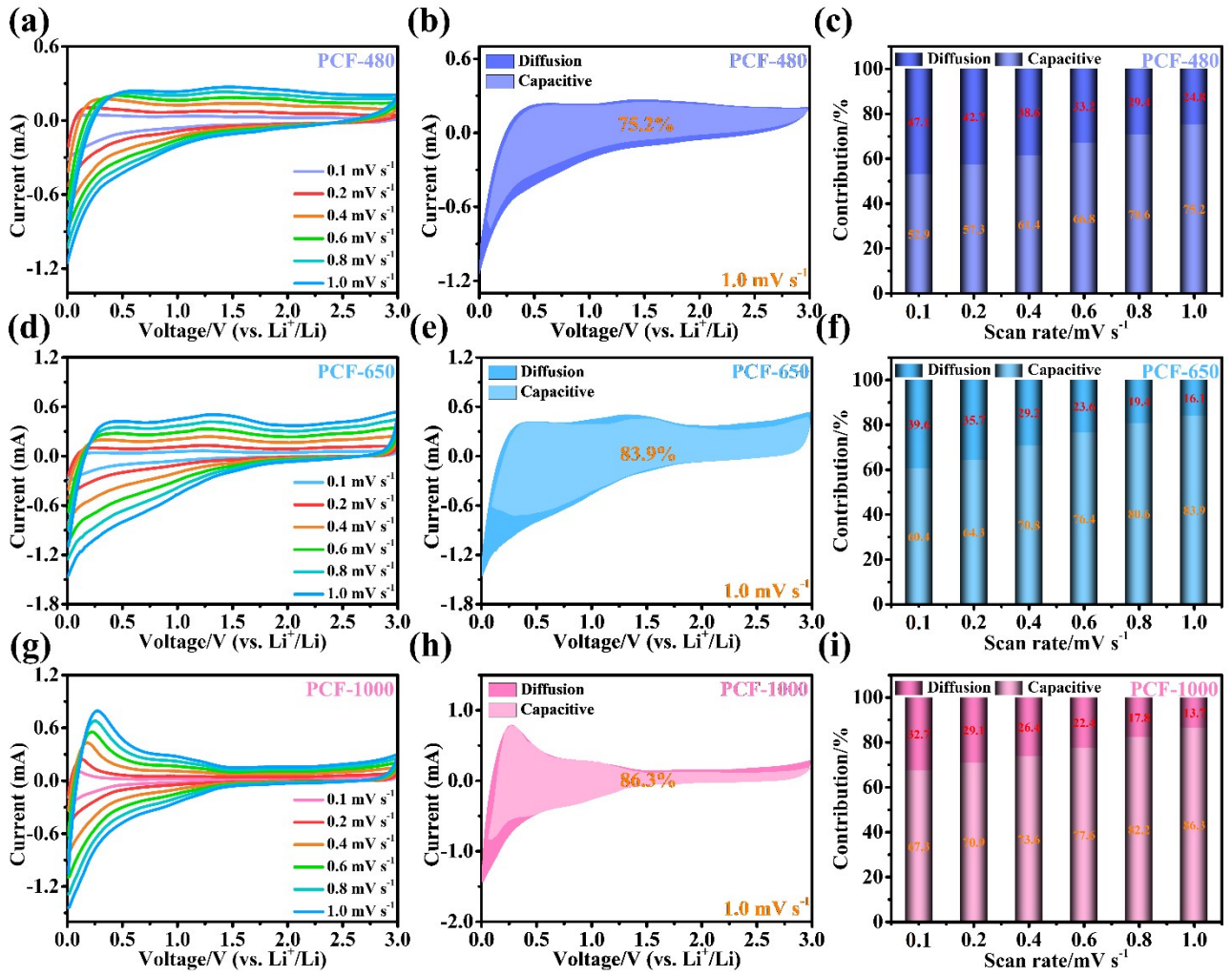

Figure S10. Electrochemical kinetics of PCF in LIBs. (a,d,g) CV curves at different scan rate from 0.1 to 1.0 mV s^{-1}. (b,e,h) capacitance contribution rate at 1.0 mV s^{-1}. (c,f,i) capacitance contribution at each scan rate.

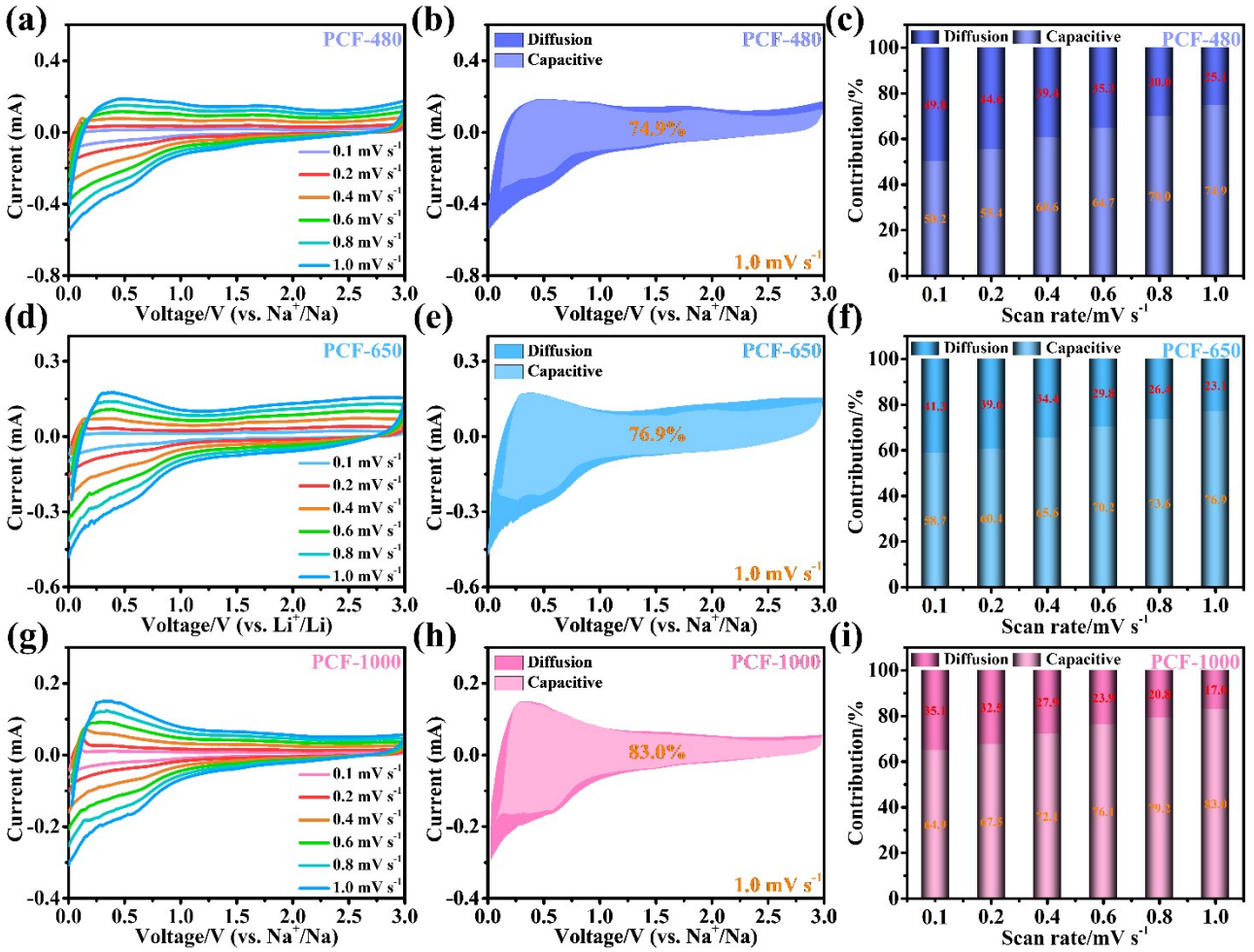

Figure S11. Electrochemical kinetics of PCF in SIBs. (a,d,g) CV curves at different scan rate from 0.1 to 1.0 mV s^{-1}. (b,e,h) capacitance contribution rate at 1.0 mV s^{-1}. (c,f,i) capacitance contribution at each scan rate.

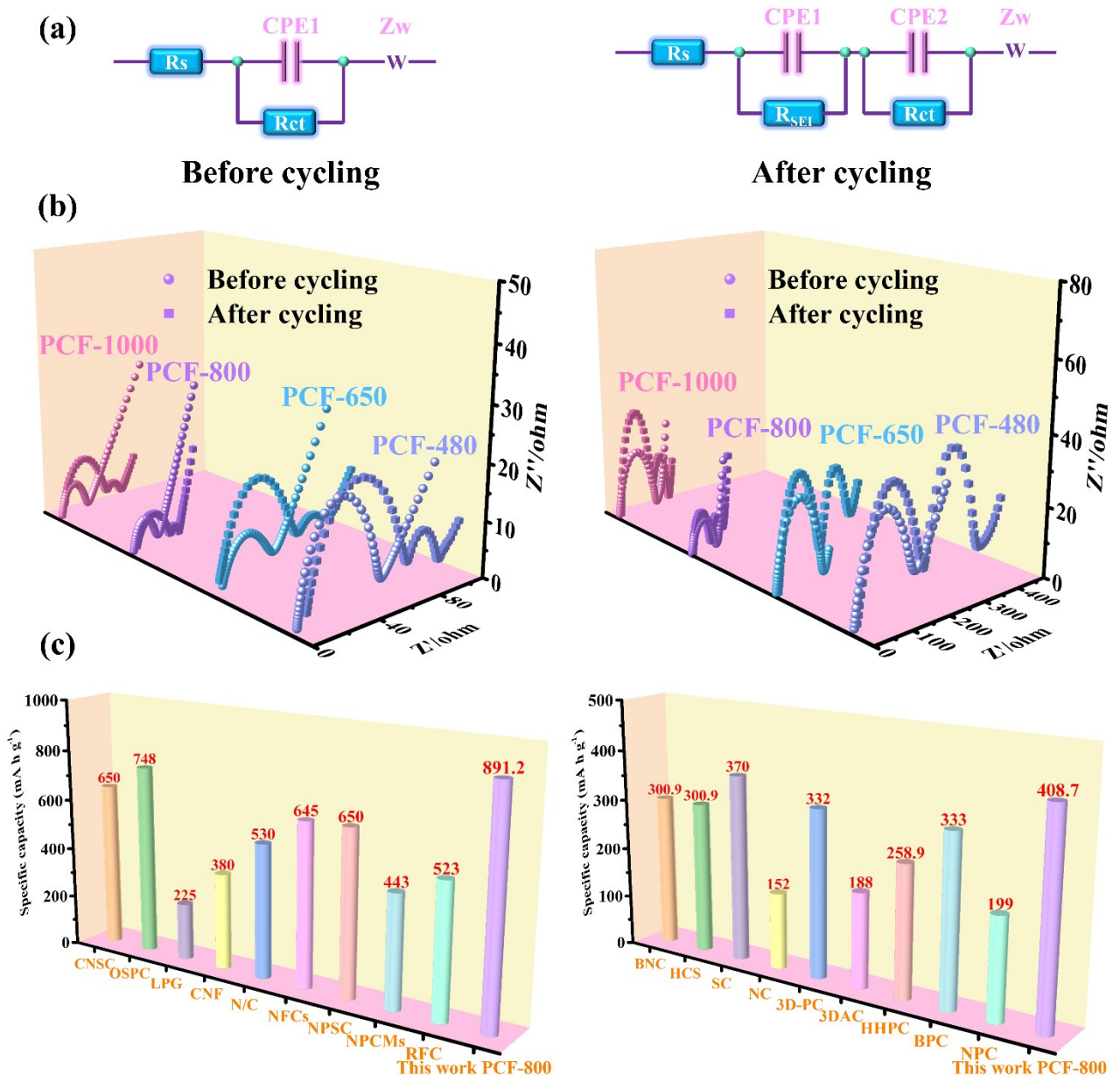

Figure S12. (a) Equivalent circuit diagram is used to fit EIS curve. (b) EIS curves of PCF before and after cycling in LIBs and SIBs. (c) Compare the cycle performance of the as-prepared PCF-800 electrode with the recently reported carbon material.

Table S5. Comparison of lithium storage performance of PCF-800 electrode with previous reports

Materials	Current density/A g^{-1}	Specific capacity/mA h g^{-1}	Cycle number
Cashewnut sheath carbon (CNSC)[9]	0.1	650	100
Polytetraethynylmethane (OSPC)[10]	0.2	748	100
Loofah-derived pseudo-graphite (LPG)[11]	0.1	225	200
Carbon nanofiber (CNF)[12]	0.1	380	200
	0.5	271	150
N-doped biomass-derived porous carbon (N/C)[13]	0.1	530	100
Nitrogen-doped 3D flower-like carbon (NFCs)[14]	0.3	645	100
	1.0	182.5	1500
N, P and S ternary-doped hierarchical porous soft carbon (NPSC)[15]	0.1	650	100
	0.5	489.5	500
Nitrogen-doped porous carbon microspheres (NPCMs) [16]	0.1	443	100
	1.0	377	500
Ramie fiber carbon (RFC)[17]	0.1	523	180
This work PCF-800	0.2	891.2	100
	1.0	509.1	1000
	5.0	416.7	1000

	10.0	333.3	1000

Table S6. Comparison of sodium storage performance of PCF-800 electrode with previous reports.

Materials	Current density/A g^{-1}	Specific capacity/mA h g^{-1}	Cycle number
B, N-co-doped carbon materials (BNC)[18]	0.1	300.9	100
Hard carbon spherules (HCS)[19]	0.1C	290	100
Sulfur-doped carbon (SC)[20]	0.2	370	100
	1.0	220	1000
Nitrogen (N)-doped carbon spheres (NC)[21]	0.05	152	200
	1.0	83	2000
Three-dimensional porous carbon (3D-PC)[22]	0.05	332	100
	5.0	120	1000
Three-dimensional amorphous carbon (3DAC)[23]	0.3	188	600
Multi-heteroatom self-doped hierarchical porous carbon (HHPC)[24]	0.02	258.9	100
	1.0	126.3	1000
Biomass porous carbon (BPC)[25]	0.1	333	400
	2.0	100	3000
N, P co-doped high-density carbon (NPC)[26]	0.1	199	150
	1.0	150	1500

This work PCF-800	0.2	408.7	100
	1.0	286.1	2000
	5.0	238.9	2000
	10.0	150.4	2000

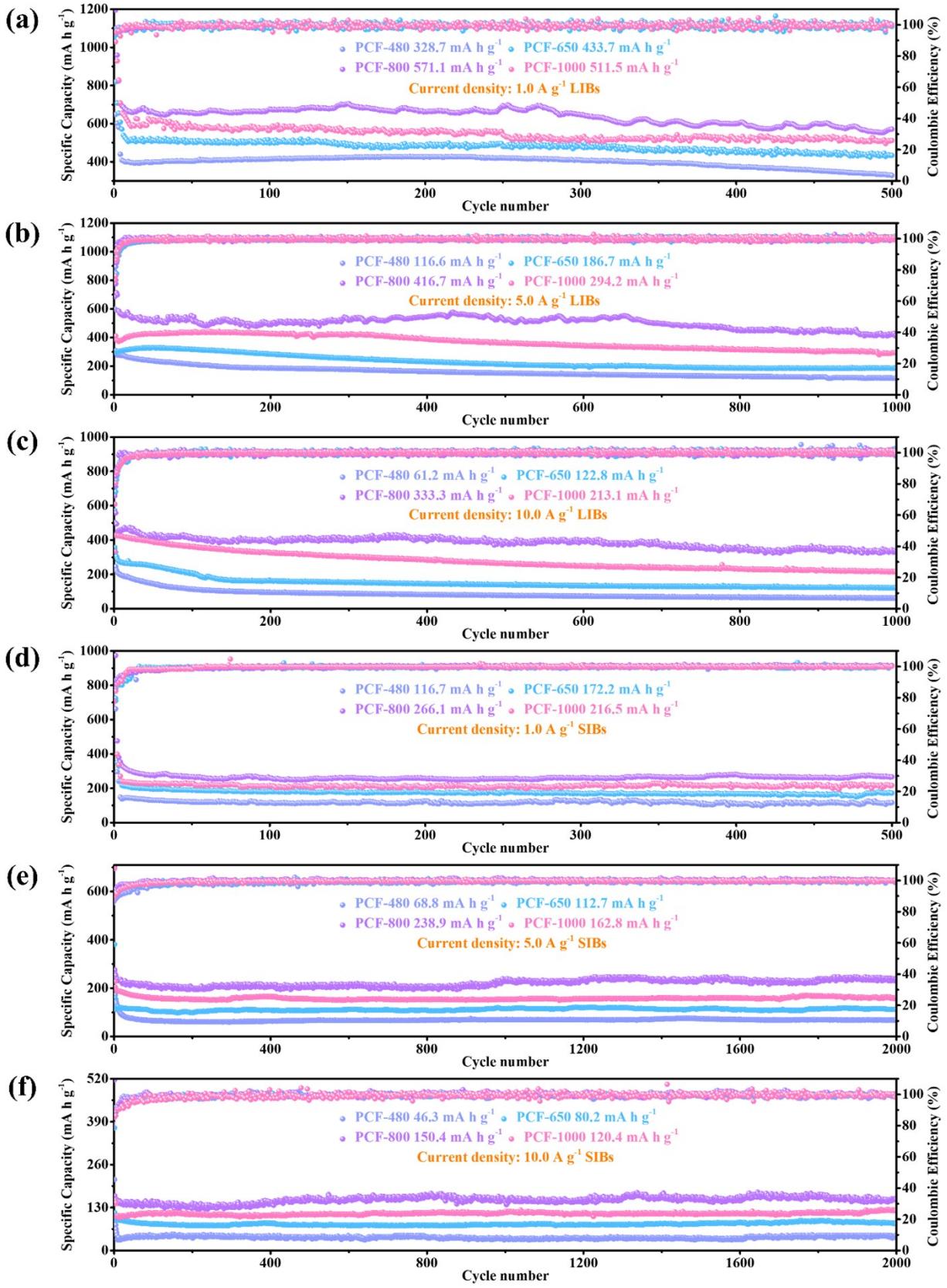

Figure S13. Cycling performances of PCF under high current density (a-c) LIBs and (d-f) SIBs.

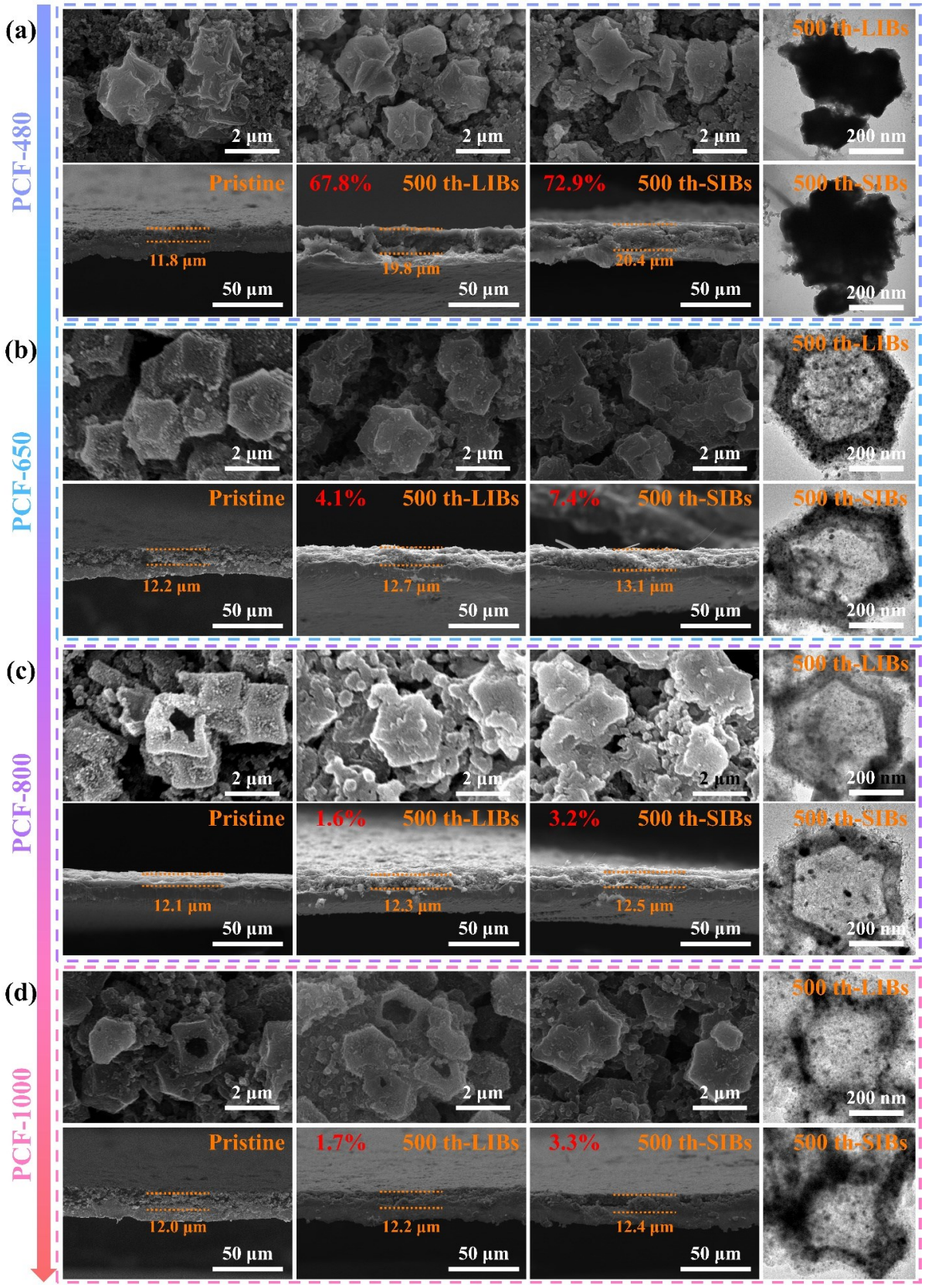

Figure S14. Structure analysis of PCF electrode before and after cycling (a) PCF-480, (b) PCF-650, (c) PCF-800 and (d) PCF -1000.

The structural effect of PCF (from solid to hollow) on the storage of Li^+/Na^+ is characterized by FESEM and TEM. The morphology and cross-sectional images of the electrode after 500 cycles at 1.0 A g^{-1} current density are shown in **Figure S14a-d** (the red numbers in the cross-sectional images indicate the volume expansion rate). The polyhedron structure of PCF-480 is severely damaged and accompanied by large volume expansion. Compared with the solid structure of PCF-480, the hollow structure of PCF has a smaller volume expansion rate. Specifically, the PCF-650 has a higher volume expansion rate than PCF-800 and PCF-1000 due to its small internal cavity. But the hollow structure can be well maintained, and the edge contour is clear. PCF-800 and PCF-1000 have relatively large internal cavities, so the volume expansion rate is approximately the same, but the edge contour of PCF-1000 has been distorted to a certain extent and the structure is unstable. In contrast, the PCF-800 is the most stable. **Figure S15a-d** collects the Raman curves after the electrode cycles. The I_D/I_G after PCF-480 cycles shows a large change, indicating that the carbon structure has undergone a large change. However, PCF-800 still showed minimal changes, which also showed the stability of the structure.

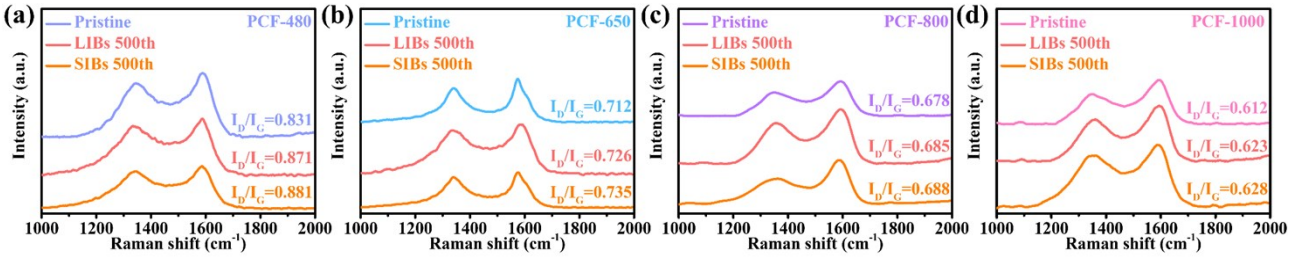

Figure S15. Raman spectra of PCF electrode before and after cycling (a) PCF-480, (b) PCF-650, (c) PCF-800 and (d) PCF -1000.

References

1. H. Pan, Z. Tan, H. Zhou, L. Jiang, Z. Huang, Q. Feng, Q. Zhou, S. Ma and Y. Kuang, *Journal of Energy Chemistry*, 2019, **39**, 101-108.

2. Z. Wang, M. Feng, H. Sun, G. Li, Q. Fu, H. Li, J. Liu, L. Sun, A. Mauger, C. M. Julien, H. Xie and Z. Chen, *Nano Energy*, 2019, **59**, 390-398.

3. H. Chen, Y. Xiao, C. Chen, J. Yang, C. Gao, Y. Chen, J. Wu, Y. Shen, W. Zhang, S. Li, F. Huo and B. Zheng, *ACS Applied Materials & Interfaces*, 2019, **11**, 11459-11465.

4. Q. Peng, F. Yu, W. Wang, A. Wang, F. Wang and Y. Huang, *Electrochimica Acta*, 2019, **299**, 749-755.

5. N. Shi, B. Xi, Z. Feng, F. Wu, D. Wei, J. Liu and S. Xiong, *Journal of Materials Chemistry A*, 2019, **7**, 4009-4018.

6. J. Lin, K. Zhang, Z. Zhu, R. Zhang, N. Li and C. Zhao, *ACS Applied Materials & Interfaces*, 2020, **12**, 2497-2504.

7. Y. Zhang, G. Xu, Q. Kang, L. Zhan, W. Tang, Y. Yu, K. Shen, H. Wang, X. Chu, J. Wang, S. Zhao, Y. Wang, L. Ling and S. Yang, *Journal of Materials Chemistry A*, 2019, **7**, 16812-16820.

8. Y. Zuo, M. Zhao, P. Ren, W. Su, J. Zhou, Y. Chen, Y. Tang and Y. Chen, *Journal of Materials Chemistry A*, 2020, **8**, 1238-1246.

9. M. Nagalakshmi and N. Kalaiselvi, *Electrochimica Acta*, 2019, **304**, 175-183.

10. Z. Zhao, S. Das, G. Xing, P. Fayon, P. Heasman, M. Jay, S. Bailey, C. Lambert, H. Yamada, T. Wakihara, A. Trewin, T. Ben, S. Qiu and V. Valtchev, *Angewandte Chemie International Edition*, 2018, **57**, 11952-11956.

11. Z. Wu, L. Wang, J. Huang, J. Zou, S. Chen, H. Cheng, C. Jiang, P. Gao and X. Niu, *Electrochimica Acta*, 2019, **306**, 446-453.

12. L. Tao, Y. Huang, Y. Zheng, X. Yang, C. Liu, M. Di, S. Larpkiattaworn, M. R. Nimlos and Z. Zheng, *Journal of the Taiwan Institute of Chemical Engineers*, 2019, **95**, 217-226.

13. H. Wan and X. Hu, *Solid State Ionics*, 2019, **341**, 115030.

14. Q. Wu, J. Liu, C. Yuan, Q. Li and H.-g. Wang, *Applied Surface Science*, 2017, **425**, 1082-1088.

15. B. Sun, Q. Zhang, H. Xiang, F. Han, W. Tang, G. Yuan, Y. Cong, C. Fan, A. Westwood and X. Li, *Energy Storage Materials*, 2020, **24**, 450-457.

16. Y. Gao, X. Qiu, X. Wang, X. Chen, A. Gu and Z. Yu, *Nanotechnology*, 2020, **31**, 155702.

17. Q. Jiang, Z. Zhang, S. Yin, Z. Guo, S. Wang and C. Feng, *Applied Surface Science*, 2016, **379**, 73-82.

18. Y. Hu, L. Shen, X. Wei, Z. Long, X. Guo and X. Qiu, *ChemistrySelect*, 2019, **4**, 6445-6450.

19. Y. Li, S. Xu, X. Wu, J. Yu, Y. Wang, Y.-S. Hu, H. Li, L. Chen and X. Huang, *Journal of Materials Chemistry A*, 2015, **3**, 71-77.

20. P. Feng, W. Wang, K. Wang, S. Cheng and K. Jiang, *Journal of Alloys and Compounds*, 2019, **795**, 223-232.

21. M. Khan, N. Ahmad, K. Lu, Z. Sun, C. Wei, X. Zheng and R. Yang, *Solid State Ionics*, 2020, **346**, 115223.

22. C. Zhou, D. Wang, A. Li, E. Pan, H. Liu, X. Chen, M. Jia and H. Song, *Chemical Engineering Journal*, 2020, **380**, 122457.

23. P. Lu, Y. Sun, H. Xiang, X. Liang and Y. Yu, *Advanced Energy Materials*, 2018, **8**, 1702434.

24. C. Chen, Y. Huang, Z. Meng, Z. Xu, P. Liu and T. Li, *Journal of Energy Chemistry*, 2021, **54**, 482-492.

25. C. Chen, Y. Huang, Y. Zhu, Z. Zhang, Z. Guang, Z. Meng and P. Liu, *ACS Sustainable Chemistry & Engineering*, 2020, **8**, 1497-1506.

26. H. Wang, H. Yuan, W. Zhan, Y.-S. Lee, H.-J. Shin, X. Wei, Q. Cai, J.-L. Lan, Y. Yu and X. Yang, *Carbon*, 2020, **165**, 204-215.